

## Back-reaction in a cylinder

J.M. Eisenberg\*

*School of Physics and Astronomy  
Raymond and Beverly Sackler Faculty of Exact Sciences  
Tel Aviv University, 69978 Tel Aviv, Israel*

*and  
TRIUMF, 4004 Wesbrook Mall, Vancouver, B.C., Canada V6T 2A3*

**Abstract:-** A system is studied in which initially a strong classical electric field exists within an infinitely-long cylinder and no charges are present. Subsequently, within the cylinder, pairs of charged particles tunnel out from the vacuum and the current produced through their acceleration by the field acts back on the field, setting up plasma oscillations. This yields a rough model of phenomena that may occur in the pre-equilibrium formation phase of a quark-gluon plasma. In an infinite volume, this back-reaction has been studied in a field-theory description, and it has been found that the results of a full calculation of this sort are well represented in a much simpler transport formalism. It is the purpose here to explore that comparison for a situation involving a cylindrical volume of given radius.

PACS numbers 11.15.Kc, 12.20.Ds

October, 1994.

\*Email: judah@giulio.tau.ac.il

## I. INTRODUCTION

The problem of back-reaction arises in a number of contexts ranging from the modeling of the pre-equilibrium phase of quark-gluon plasma production [1,2] to studies of inflationary cosmology [3-5]. In general terms, back-reaction consists in a situation where a system can be viewed as governed by the mutual interaction between a field, usually taken as classical, and pairs of charged particles that are produced through its presence. In one version, the initial condition posits the pre-existence of the field and an approximate vacuum insofar as the particles are concerned. Pairs can then tunnel out of this vacuum by reason of their interaction with the field in a purely quantal process. These pairs are accelerated by the field, producing a current which in turn acts back on the field. The back-reaction leads to plasma oscillations as one of its key characteristic effects.

Within the past few years, it has proved possible to carry out detailed calculations for back-reaction in which boson [6] or fermion [7] pairs are produced, including the case where boost-invariant coordinates are used [8] as is appropriate for the study of the quark-gluon plasma. (See also the didactic article in Ref. [9] and the review in Ref. [10].) Somewhat surprisingly, it has emerged that calculations [1,2] based on the much simpler transport formalism follow the field-theory results in detail provided that quantum fluctuations are smoothed and quantum statistical effects are introduced into the transport equations [6-10]. That is, it proves possible to mimic the quantum tunneling through the use of a source term based on the Schwinger mechanism [11] in a transport equation. The squares of the quantal mode amplitudes, describing the momentum distribution of the produced pairs, even agree remarkably closely with the corresponding transport-function momentum dependence once smoothing and statistics are included. There are also formal derivations [12,13] of the mapping from field theory to transport formalism in this context, providing [13], for example, an understanding of how nonmarkovian features enter the theory. Thus the back-reaction problem provides a model of a system sufficiently simple that the nonperturbative field-theory description can be fully solved numerically and approximations to it—notably the transport formalism—can be studied in detail, but with enough complexity to allow for a richness of phenomena and features. This is especially interesting when the nonequilibrium thermodynamics of back-reaction is considered [8]. The field-theory version then refers to the time evolution of a pure quantum state, while the transport formalism has a well-defined entropy which increases with time.

One may also hope that essential features of the quark-gluon plasma lacking in this simple back-reaction model will eventually be incorporated and their effects studied. These must surely include (i) the nonabelian nature of quantum chromodynamics which governs the plasma; (ii) the nonclassical nature of the chromoelectric field that enters there; and (iii) the fact that the plasma lives in a finite volume, not in the infinite volume treated so far in back-reaction. To the degree that a mapping from field theory to transport formalism can be found, say, in the presence of each of these features separately, the use of the relatively simple transport formalism for the description of the plasma gains considerable support. Towards this end, some progress has been made in the formulation of back-reaction for the nonabelian Yang-Mills case [14]; a detailed study [15] has been carried out for the lowest quantal correction to the classical electric field used so far; and it is the purpose of this paper to study back-reaction in a (transversely) finite volume of a geometry chosen for its eventual applicability to the quark-gluon plasma.

We consider back-reaction in an infinitely-long cylindrical sleeve, as shown in Figure 1, for an abelian and classical electromagnetic field. The choice of a volume whose finiteness is only in the direction transverse to that of the electric field and particle current was made with a view to eventual extension to the quark-gluon plasma, where boost-invariant coordinates would be used for the longitudinal variables. (In one spatial dimension, the case of back-reaction on a finite line segment has been considered [16] in the past.) The symmetry here about the cylindrical axis is, of course, a sizable simplification for our problem, though it still leaves in it the complexities of mode mixing and of renormalization, and appears to be just barely amenable to handling at the numerical level with present 100-MHz or 150-MHz computer processors. We develop below the formalism for back-reaction in this geometry, first for field theory and then for the transport formalism, then discuss briefly numerical methods and approximations for each, and compare results for the two approaches.

## II. FIELD-THEORY FORMALISM

We consider QED for scalar particles of charge  $e$  and mass  $m$ , governed by the Klein-Gordon equation

$$[(\partial^\mu + ieA^\mu)(\partial_\mu + ieA_\mu) + m^2]\Phi = 0, \quad (1)$$

coupled with the classical Maxwell equation

$$\left(\frac{\partial^2}{\partial t^2} - \nabla^2\right)A^\mu = \langle j^\mu \rangle. \quad (2)$$

Here  $A^\mu$  is the classical four-vector potential and  $j^\mu$  is the four-current, taken in an expectation value for some initial configuration of the charges. The current is given by

$$\begin{aligned} j^\mu = & \frac{1}{2}ie\{\Phi^\dagger(\partial^\mu + ieA^\mu)\Phi - [(\partial^\mu + ieA^\mu)\Phi]^\dagger\Phi \\ & - \Phi[(\partial^\mu + ieA^\mu)\Phi]^\dagger + [(\partial^\mu + ieA^\mu)\Phi]\Phi^\dagger\}, \end{aligned} \quad (3)$$

in terms of a second-quantized field  $\Phi$ .

We choose the geometry of an infinite cylinder of radius  $R$  (see Figure 1) and restrict the initial conditions to be independent of the polar angle  $\varphi$  and assume that initially there are no regions of nonvanishing net charge  $j^0(\mathbf{r}, t)$  and that the initial field configuration consists of  $\mathbf{E}(b, t) \parallel \hat{\mathbf{z}}$ , where  $b = |\mathbf{b}|$  is the radial coordinate. The current  $\mathbf{j}(\mathbf{r}, t)$  then remains parallel to the axis of the cylinder  $\hat{\mathbf{z}}$ . This is because (see Figure 1) the opposite charges of a produced pair are accelerated by  $\mathbf{E}$  in opposite directions parallel to  $\hat{\mathbf{z}}$ . The magnetic field  $\mathbf{B}(b, t)$  that is produced has solenoidal geometry, whence both the positive and the negative charges undergo transverse acceleration of the same direction and magnitude, canceling any transverse contribution to the current. Selecting a gauge such that  $A^\mu = (0; 0, 0, A(b, t))$  has a  $z$ -component only, the Klein-Gordon equation becomes

$$\left[\frac{\partial^2}{\partial t^2} - \nabla_\perp^2 - \left(\frac{\partial}{\partial z} - ieA(b, t)\right)^2 + m^2\right]\Phi(b, \varphi, z; t) = 0, \quad (4)$$

where

$$\nabla_\perp^2 = \frac{\partial^2}{\partial b^2} + \frac{1}{b} \frac{\partial}{\partial b} + \frac{1}{b^2} \frac{\partial^2}{\partial \varphi^2}. \quad (5)$$

We choose boundary conditions such that there are no particles on or outside the cylinder wall at  $b = R$ ; the electric field is also taken to vanish at and

beyond  $b = R$ . These are boundary conditions appropriate to electromagnetism. One could of course choose bag boundary conditions in their place. In expanding  $\Phi$  over creation and annihilation operators, we then use the orthonormal basis set

$$\phi_{ln}(\mathbf{b}) = \frac{e^{il\varphi}}{\sqrt{2\pi}} \frac{\sqrt{2}}{R} \frac{J_l(k_{\perp}(ln)b)}{J'_l(k_{\perp}(ln)R)}, \quad (6)$$

where  $k_{\perp}(ln) = z_{ln}/R$ ,  $z_{ln}$  being the  $n$ th zero of the Bessel function of order  $l$ . In the following, we indicate the pair  $\{l, n\}$  by  $n$ ; the lack of  $\varphi$ -dependence restricts our interest to  $l = 0$  in any event. Then

$$\Phi = \sum_n \int_{-\infty}^{\infty} \frac{dk}{2\pi} \phi_n(b) \frac{e^{ikz}}{(2\omega_{k,n}^0)^{1/2}} [a_{k,n}(t) + b_{-k,n}^{\dagger}(t)], \quad (7)$$

where  $a_{k,n}$  annihilates particles of longitudinal momentum  $k$  and radial mode  $n$ ,  $b_{-k,n}^{\dagger}$  creates antiparticles with  $-k$  and  $n$ , and  $\omega_{k,n}^0 = [k^2 + k_{\perp}^2(n) + m^2]^{1/2}$ . The usual commutators pertain,

$$[a_{k,n}(t), a_{k',n'}^{\dagger}(t)] = [b_{k,n}(t), b_{k',n'}^{\dagger}(t)] = 2\pi\delta(k - k')\delta_{n,n'}, \quad (8a)$$

$$[a_{k,n}(t), b_{k',n'}^{\dagger}(t)] = 0, \quad (8b)$$

and so forth. We must relate these operators to their values at  $t = 0$ , which we do by means of a Bogolyubov transformation [17]

$$a_{k,n}(t) = \sum_{n'} [u_{k,nn'}(t)a_{k,n'}(0) + v_{k,nn'}(t)b_{-k,n'}^{\dagger}(0)], \quad (9a)$$

and

$$b_{-k,n}^{\dagger}(t) = \sum_{n'} [v_{k,nn'}^*(t)a_{k,n'}(0) + u_{k,nn'}^*(t)b_{-k,n'}^{\dagger}(0)], \quad (9b)$$

where

$$u_{k,nn'}(0) = \delta_{nn'}, \quad v_{k,nn'}(0) = 0, \quad (9c)$$

$$\sum_{\bar{n}} [u_{k,n\bar{n}}(t)u_{k,n'\bar{n}}^*(t) - v_{k,n\bar{n}}(t)v_{k,n'\bar{n}}^*(t)] = \delta_{nn'}, \quad (9d)$$

and

$$\sum_{\bar{n}} [u_{k,n\bar{n}}(t)v_{k,n'\bar{n}}(t) - v_{k,n\bar{n}}(t)u_{k,n'\bar{n}}(t)] = 0, \quad (9e)$$

in an obvious extension of the usual [17] forms.

Defining the mode amplitudes

$$f_{k,nn'}(t) = \frac{1}{(2\omega_{k,n}^0)^{1/2}} [u_{k,nn'}(t) + v_{k,nn'}^*(t)], \quad (10a)$$

with the initial values

$$f_{k,nn'}(0) = \frac{1}{(2\omega_{k,n}^0)^{1/2}} \delta_{nn'}, \quad \dot{f}_{k,nn'}(0) = -i \left( \frac{\omega_{k,n}^0}{2} \right)^{1/2} \delta_{nn'}, \quad (10b)$$

the scalar field becomes

$$\Phi = \sum_{nn'} \int_{-\infty}^{\infty} \frac{dk}{2\pi} e^{ikz} \phi_n(b) [f_{k,nn'}(t) a_{k,n'}(0) + f_{k,nn'}^*(t) b_{-k,n'}^\dagger(0)]. \quad (11)$$

The normalization of the mode amplitudes in Eqs. (10) is taken so as easily to accommodate the canonical commutation relations

$$[\Phi(\mathbf{r}, t), \Pi(\mathbf{r}', t)] = i\delta(\mathbf{r} - \mathbf{r}'), \quad (12)$$

where  $\Pi = \dot{\Phi}$  is the field conjugate to  $\Phi$ . Equation (12), with the commutators of Eqs. (8), leads, among other similar relations, to the wronskian condition for the mode amplitudes,

$$\sum_{\bar{n}} [f_{k,n\bar{n}}(t) \dot{f}_{k,n'\bar{n}}^*(t) - f_{k,n\bar{n}}^*(t) \dot{f}_{k,n'\bar{n}}(t)] = i\delta_{nn'}, \quad (13)$$

which is guaranteed by the dynamics to be satisfied at all times if it is fulfilled initially, as it is of course by Eq. (10b).

Substituting Eq. (11) into Eq. (4) yields the dynamical equations for the mode amplitudes

$$\ddot{f}_{k,nn'}(t) + \sum_{\bar{n}} \langle n | \omega_k^2(t) | \bar{n} \rangle f_{k,\bar{n}n'}(t) = 0, \quad (14a)$$

where

$$\begin{aligned} \langle n | \omega_k^2(t) | \bar{n} \rangle &= \int d\mathbf{b} \phi_n^* \omega_k^2(\mathbf{b}, t) \phi_{\bar{n}} \\ &= \int d\mathbf{b} \phi_n^* \{ (k - eA(b, t))^2 + k_\perp^2(n) + m^2 \} \phi_{\bar{n}}. \end{aligned} \quad (14b)$$

For our geometrical conditions and with the assumption that the initial charge configuration in Eq. (2) is the adiabatic vacuum, annihilated by  $a_{k,n}(0)$  and by  $b_{k,n}(0)$ , the expectation value of the current becomes

$$\begin{aligned} \langle j \rangle &= e \int \frac{dk}{2\pi} (k - eA(b, t)) \sum_{nn'} \phi_n(b) \phi_{n'}^*(b) \\ &\quad \times \sum_{\bar{n}} [f_{k,n'\bar{n}}^*(t) f_{k,n\bar{n}}(t) + f_{k,n'\bar{n}}(t) f_{k,n\bar{n}}^*(t)]. \end{aligned} \quad (15)$$

As is well known (see, e.g., the broad discussion in Ref. [17]), the current in Eq. (15) suffers from divergences. For the case of infinite volume, this has been dealt with systematically through the procedure of adiabatic regularization [17]. Unfortunately, that is inapplicable here because of the mode mixing inherent in our problem and explicit in Eqs. (14). We therefore follow an alternative strategy here. First we consider the high-momentum limit ( $k \rightarrow \infty$ ,  $n \rightarrow \infty$ ) for  $f_{k,nn'}(t)$  satisfying the dynamical equations (14) and the wronskian condition (13). A direct generalization of the usual WKB approach [17] suggests

$$f_{k,n'n}(t) \longrightarrow \langle n' | \frac{\exp[-i \int^t \omega_k(t') dt']}{\sqrt{2\omega_k(t)}} | n \rangle, \quad (16)$$

as  $k, n, n' \rightarrow \infty$ , where we restrict ourselves to the leading term of the WKB since the higher-order refinements are of no use in the presence of mode mixing. It is easily seen that this form satisfies Eq. (13) exactly and Eqs. (14) through order  $k^0$ . To study the worst divergence in Eq. (15), we substitute this into the factor involving a summation over  $n, n'$ , and  $\bar{n}$  there to obtain, using closure,

$$\begin{aligned} \sum_{nn'} \phi_n(b) \phi_{n'}^*(b) \cdot 2\pi \int_0^\infty b' db' \phi_n^*(b') \frac{1}{\omega_k(b', t)} \phi_{n'}(b') = \\ = \sum_n \phi_n(b) \phi_n^*(b) \frac{1}{\omega_k(b, t)}, \end{aligned} \quad (17)$$

where we again used closure to obtain the last line. It is then easy to see that this divergent form in fact vanishes upon symmetric integration [10,17] in Eq. (15). This identifies the worst, cubic divergence there, which is dealt with by subtracting the form of (17) to arrive at

$$\begin{aligned} \langle j \rangle = e \int_{-\infty}^\infty \frac{dk}{2\pi} (k - eA(b, t)) \sum_{nn'} \phi_n(b) \phi_{n'}^*(b) \\ \times \left\{ \sum_{\bar{n}} [f_{k,n'\bar{n}}^* f_{k,n\bar{n}} + f_{k,n'\bar{n}} f_{k,n\bar{n}}^*] - \frac{\delta_{nn'}}{\omega_k(b, t)} \right\}. \end{aligned} \quad (18)$$

This expression still contains, of course, the usual logarithmic divergence of charge renormalization, dealt with in adiabatic regularization [10,17] by considering higher-order WKB than shown in Eq. (16). This is what does not go through in the mode-mixed case. Instead, we base ourselves on the expectation that charge renormalization is what must emerge in any event. This is shown explicitly for adiabatic regularization in the infinite volume in Ref. [17], and we

do not expect a change in high-momentum, short-interval behavior here merely because of the presence of the cylinder walls. Thus we calculate Eq. (18) with a  $k$ -momentum cutoff  $\Lambda$  and a radial mode cutoff  $n_{max}$ , at the same time replacing the charge  $e$  by the renormalized charge

$$\sqrt{Z}e = e(1 + e^2 \delta e^2)^{-1/2} = e \left[ 1 + \frac{e^2}{24\pi^2} \log \left( \frac{1}{m} (\Lambda^2 + \pi^2 n_{max}^2 / R^2)^{1/2} \right) \right]^{-1/2}, \quad (19)$$

and testing that results are insensitive to  $\Lambda$  and  $n_{max}$ .

Equation (18) is now used in Eq. (2) as

$$\left( \frac{\partial^2}{\partial t^2} - \nabla_{\perp}^2 \right) A(b, t) = \langle j(b, t) \rangle \quad (20)$$

for the dynamics of the electromagnetic field. The coupled equations that must be solved for the field-theory study of back-reaction in an infinitely-long cylinder are then Eqs. (14), (18), and (20).

### III. TRANSPORT FORMALISM

The transport equation we must deal with in the presence of the cylindrical symmetry of Figure 1 is, for a positive charge  $e$ ,

$$\begin{aligned} \frac{\partial}{\partial t} f(\mathbf{b}; \mathbf{p}; t) + \frac{\mathbf{p}_{\perp}}{\mathcal{E}} \cdot \frac{\partial}{\partial \mathbf{b}} f(\mathbf{b}; \mathbf{p}; t) \\ + e \left( \mathbf{E} + \frac{\mathbf{p}}{\mathcal{E}} \times \mathbf{B} \right) \cdot \left( \frac{\partial}{\partial \mathbf{p}_{\perp}} + \hat{\mathbf{z}} \frac{\partial}{\partial p_{\parallel}} \right) f(\mathbf{b}; \mathbf{p}; t) = S\{E, B; \mathbf{p}\}, \end{aligned} \quad (21)$$

where  $f$  is the transport function and  $S$  is a source function based on the Schwinger mechanism for pair production in a fixed field. The spatial variable  $\mathbf{b}$  is, as hitherto, the transverse position measured from the cylinder axis; again there is no  $z$ -dependence here. The momentum  $\mathbf{p} = \{\mathbf{p}_{\perp}, p_{\parallel}\}$  is taken in terms of a transverse component  $\mathbf{p}_{\perp}$  and a longitudinal one  $p_{\parallel}$ , while  $\mathcal{E} = (\mathbf{p}_{\perp}^2 + p_{\parallel}^2 + m^2)^{1/2}$  is the particle energy. Note that with our geometry there can be dependence only on an azimuthal angle  $\varphi$ , the angle between  $\mathbf{b}$  and  $\mathbf{p}_{\perp}$ . In parallel to the field case of the previous section, we impose the boundary condition  $f(b = R; \mathbf{p}_{\perp}, p_{\parallel}; t) = 0$ . Given the field configuration discussed in the previous section and shown in Figure 1, the transport equation (21) takes on the form

$$\frac{\partial f}{\partial t} + \frac{\mathbf{p}_{\perp}}{\mathcal{E}} \cdot \frac{\partial f}{\partial \mathbf{b}} + e \left[ E \frac{\partial}{\partial p_{\parallel}} + \left( \frac{\mathbf{p}_{\perp}}{\mathcal{E}} \times \mathbf{B} \right) \cdot \hat{\mathbf{z}} \frac{\partial}{\partial p_{\parallel}} + \left( \frac{p_{\parallel}}{\mathcal{E}} \hat{\mathbf{z}} \times \mathbf{B} \right) \cdot \frac{\partial}{\partial \mathbf{p}_{\perp}} \right] f = S. \quad (22)$$



Negative charges move in accordance with Eq. (21) or (22), but with  $e$  replaced by  $-e$ . Since the source term depends only on  $|e|$ , it follows from Eq. (22) that the transport function for negative charges is given by that for positive charges with  $p_{\parallel} \rightarrow -p_{\parallel}$ .

The source term in Eq. (21) or (22) is taken as [6-10]

$$S\{E, B; \mathbf{p}\} = \delta(p_{\parallel})|e|\sqrt{E^2 - B^2} \log \left[ 1 + \exp \left( - \frac{\pi(\mathbf{p}_{\perp}^2 + m^2)}{|e|\sqrt{E^2 - B^2}} \right) \right], \quad (23)$$

where we insist that the invariant  $E^2 - B^2$  be timelike, so that energy considerations allow pairs to be produced, taking  $S = 0$  for  $B \geq E$ . In Eq. (23), the usual choice [6-10,12] has been made to the effect that the particles are produced at zero longitudinal momentum. A study based on the projection method [13] has found that the source term is well localized around  $p_{\parallel} \sim 0$  for rather large fields,  $e\sqrt{E^2 - B^2}/\sqrt{\mathbf{p}_{\perp}^2 + m^2} > 1$  in our notation; this situation is, in fact, the only one considered here. Since our results depend ultimately on the pair current, which involves an integration over  $p_{\parallel}$ , they prove to be very insensitive to the appearance of  $\delta(p_{\parallel})$  in  $S$ , being essentially unchanged for distributions in  $p_{\parallel}$  centered around  $p_{\parallel} = 0$ , normalized with respect to integration over  $p_{\parallel}$  as is  $\delta(p_{\parallel})$ , and with widths ranging up to several times  $m$ . The nonmarkovian features found in Ref. [13] also disappear, of course, with the source term of Eq. (23), in consonance with the findings of Ref. [13] for large fields. Last, we shall not consider here the consequences of Bose enhancement in the transport equation treatment, the general effects being well known from previous work [6,10]; to deal with such enhancement for the finite-volume case would require some selection of cell size in phase space within which statistical effects would take place.

The nontrivial Maxwell equations in our geometry are

$$\frac{\partial B}{\partial t} = \frac{\partial E}{\partial b} \quad \text{and} \quad \frac{\partial E}{\partial t} = -j + \frac{1}{b} \frac{\partial}{\partial b}(bB), \quad (24a, b)$$

where  $j$  is the current—again purely longitudinal—given by a conduction and a polarization part,

$$j(b, t) = j_{\text{cond}}(b, t) + j_{\text{pol}}(b, t), \quad (25a)$$

where

$$j_{\text{cond}}(b, t) = 2e \int \frac{d\mathbf{p}}{(2\pi)^3} \frac{p_{\parallel}}{\mathcal{E}} f(\mathbf{b}, \mathbf{p}; t) \quad (25b)$$

and

$$j_{\text{pol}}(b, t) = \frac{2}{E} \int \frac{d\mathbf{p}}{(2\pi)^3} \mathcal{E}S\{E, B; \mathbf{p}\}. \quad (25c)$$

The coupled equations that must be solved for the transport-theory study of back-reaction are then Eqs. (22), (24), and (25).

#### IV. NUMERICAL PROCEDURES

We discuss first the procedures for the field-theory formulation. Since the three-dimensional studies of back-reaction in an infinite volume proved taxing from the computational point of view [10], it was, of course, to be expected that the finite-volume case would present difficulties in terms of the length of processor time required, and this was indeed the case. The infinite-volume calculation required very refined grids for the time variable (typically the time step was on the order of  $10^{-4} m^{-1}$ ) and longitudinal momentum (typically requiring some  $10^3$  points). The renormalization scheme used here [see Eq. (19) and the discussion surrounding it] is, however, simpler than the iterative one used for infinite volume [10].

Numerical procedures were straightforward: the current  $j(b, t)$  and potential  $A(b, t)$  and field  $E(b, t)$  were all expanded in terms of the basis set of Eq. (6). The initial field was usually taken in the form

$$E(b, 0) = E_0 J_0(z_{00}b/R), \quad (26)$$

in the notation of Section II. The mode amplitudes  $f_{k,nn'}(t)$  were then calculated from the coupled ordinary differential equations (14) using Runge-Kutta and the Fourier-Bessel components of the current  $j(b, t)$  were evaluated by Simpson integration of Eq. (18). The subtraction of the counter term in (18) required a return to configuration space for the evaluation of  $\omega_k^{-1}(b, t)$ . The Fourier-Bessel components of the potential and field were then advanced using Eq. (20)—again an ordinary differential equation in the transform space—with Runge-Kutta. Thus worries about possible instabilities in partial differential equations were avoided.

The rapid fluctuations encountered in the mode amplitudes in the infinite-volume case seem here to translate into a great deal of mode coupling in the finite volume, with a consequent need for a large number of Fourier-Bessel components in order to represent the current adequately. We here worked typically with about 500 longitudinal momentum points and summed  $n$  out to about  $n_{max} \sim 20$ . Time

steps again had to be kept small ( $dt \sim 10^{-4}$ ). Since computation times rise quartically, or faster, with  $n_{max}$ , this led to runs of several weeks with a 100-MHz or 150-MHz processor. Moreover, as for infinite volume, quantum fluctuations will eventually be more rapid than can be accommodated by any grid choice, so that our computation scheme must eventually break down. Confidence in the validity of the field calculation is therefore partly based on the usual tests checking that results do not change appreciably when grid sizes are refined. It also partly derives from the qualitative and even semiquantitative agreement between field and transport methods over the time range we treat, a comparison which is, of course, the primary goal of this study.

Somewhat surprisingly, the transport formalism is also somewhat tedious computationally. The infinite-volume case allowed for solution of the transport equations using essentially an analytic scheme based on the method of characteristics [10], but for a finite volume we had to solve Eq. (22) as a partial differential equation, using a Lax method [18]. Other methods, such as Lax-Wendroff or staggered leapfrog seemed to offer little improvement over this. The time evolution of the electromagnetic fields as partial differential equations (24)—even in the absence of a current  $j$ —proved unstable and this was not easily cured through the use of Lax, Lax-Wendroff, or leapfrog methods, so we again resorted to Fourier-Bessel decomposition and advanced the coefficients in time using a predictor-corrector method. The time increment was again  $dt \sim 10^{-4}$  and roughly 120 longitudinal momentum points were required. In the transverse direction about 120 momentum points and 80 spatial points were needed.

The outcome of all this was again very long computation time. The situation was eased somewhat by great insensitivity to the treatment of the angular variable  $\varphi$ . Eventually we chose to average over this, fixing  $\varphi = \pi/2$ . This changed the results typically by only a few percent. We also eventually averaged the transverse momentum  $|\mathbf{p}_\perp|$  in a manner suggested by the gaussian dependence of the source term of Eq. (23), taking  $\langle p_\perp \rangle = (\sqrt{\pi|e|}/2)(E^2 - B^2)^{1/4}$ . This approximation reproduced very well the amplitudes and frequencies of the oscillatory behavior of  $j(b, t)$  and  $E(b, t)$ , but was clearly deficient near the zeros of these quantities, where it led to a flattening or step in  $j$  near its zeros.

## V. RESULTS AND DISCUSSION

In presenting results in Figures 2 through 13, all quantities are given in natural units, so that spatial coordinates are measured in  $1/m$  and momentum coordinates in  $m$ . The electromagnetic four-potential is presented as  $a(b, t) = eA(b, t)/m^3$ , the electric field as  $e(b, t) = eE(b, t)/m^4$ , and the current as  $j(b, t) \rightarrow ej(b, t)/m^5$ . The cases chosen for presentation here parallel parameter sets picked in the study of the infinite-volume situation [10]. We shall generally show the current and the electric field averaged over the cylinder cross section according to

$$Q(t) \equiv \frac{1}{\pi R^2} \int_0^\infty d\mathbf{b} q(\mathbf{b}, t), \quad (27)$$

where  $q(\mathbf{b}, t) = j(\mathbf{b}, t)$  or  $e(\mathbf{b}, t)$ . This, as we shall see, converges much faster as the number of Fourier-Bessel components  $n_{max}$  is increased than do, say, the on-axis values.

Figures 2 and 3 present the transversely-integrated current and electric field for unrenormalized charge  $e^2 = 10$ , on-axis initial electric field  $e(b = 0, t = 0) = 6$ , and cylinder radii  $R = 2$  and  $5$ . The large value of the charge chosen here has the advantage, given our need for very lengthy computer time, that back-reaction effects have a chance to make themselves felt within the relatively short time interval  $t < 4$  (see Ref. [10]). As will be generally true below, the electric field integrated over the cylinder cross section is very similar for the field-theory approach and the transport calculation. Of course, this is partly the case because, for the small radii considered here, the electric field oscillations are largely driven by cylinder radius, not by back-reaction. Thus, by  $R = 10$  this agreement begins to break down. On the other hand,  $R = 10$  stretches the range of reliability of our calculation, since we must require that the ‘‘transverse momentum’’  $n_{max}\pi/R$  be on the order of 10 to 20 in order to cover the relevant momentum distributions and to yield a valid regularization scheme using Eq. (18). Since in practice we are limited to  $n_{max} \leq 20$ , this implies a breakdown in our procedures for  $R$  much beyond 5 or so. The transversely-integrated currents as calculated from field theory are substantially more oscillatory than their transport-theory counterparts, which is not surprising in view of the infinite-volume results [10]. The initial sharp rise in the current occurs in both cases, though with rather different values; thereafter there is reasonable similarity between the two methods if one takes into account an effective time-averaging over the field-theory fluctuations. It is worth noting

[19] that the initial rapid variations in the electric field in the quantal case may “shake off” charges by means of the fast fluctuations, an effect not included in the transport approach here, where only pair tunneling is included.

In an attempt to make some connection with the infinite-volume results, we show  $j$  and  $e$  on the cylinder axis for  $e^2 = 10$ , initial field  $e(b = 0, t = 0) = 6$ , and  $R = 2$  and  $5$  in Figures 4 and 5. Agreement here between field theory and transport formalism is much less satisfactory than the situation for the integrated values: The electric field on-axis remains similar for the two cases, again because its values are essentially determined by the initial condition and the cylinder radius, but the current differs by nearly two orders of magnitude. This is almost certainly in large part a numerical breakdown brought about by the difficulty in using a large enough number of Fourier-Bessel components to achieve reliable results for the on-axis case. (For Figures 2 through 5 we used  $n_{max} = 20$ .) Since  $J_0(0) = 1$ , all the components add coherently to produce the  $b = 0$  values, and thus these are very sensitive to limitations in  $n_{max}$ . On the other hand, the on-axis value of the current is weighted with a factor of  $b$  and hence does not really contribute when global features are considered.

The corresponding picture for a smaller charge, namely,  $e^2 = 4$ , with initial field  $e(b = 0, t = 0) = 7$ , and again for  $R = 2$  and  $5$  is shown in Figures 6 through 9 (where we have worked with  $n_{max} = 10$  in order to allow for the calculation to extend out to  $t = 30$ , and encompass several cycle times). As is known from the infinite-volume case [10], the field-theory and transport-formalism results eventually drift out of phase, a condition that would be improved by incorporating Bose enhancement into the transport equation [10]. Again, if one were to average over the fluctuations present in each cycle of the current, agreement between the two methods is quite reasonable for the integrated values, and not very good for on-axis results.

In Figures 10 and 11 we compare, for  $e^2 = 10$ ,  $e(b = 0, t = 0) = 6$ , and  $R = 2$  and  $5$ , results for two different numbers of Fourier-Bessel components,  $n_{max} = 10$ ,  $dt = 2 \times 10^{-4}$ , 401  $k$ -grid points, and  $\Lambda = 20$  (dashed curve) vs.  $n_{max} = 20$ ,  $dt = 10^{-4}$ , 1,001  $k$ -grid points, and  $\Lambda = 40$  (solid curve) for the transversely-integrated current and electric field. The same comparisons for the on-axis quantities are shown in Figures 12 and 13. Since we have here a doubling in this upper limit for the number of transverse modes  $n_{max}$ , the rea-

sonable agreement for the integrated values suggests that the results there for  $n_{max} = 20$  are quantitatively reliable. Obviously this is not yet the case for the on-axis quantities—notably the current, which differs by two orders of magnitude for  $t > 2$ —which at best have qualitative validity. It is perhaps not surprising that the less numerically reliable field-theory result (dashed curve) more closely resembles the transport calculation, since its inferior numerics automatically perform some sort of average over the quantal fluctuations of the field-theory result. Such an averaging would otherwise only properly be performed by doing the field-theory computation with much more refined parameters than are presently accessible and then averaging these results over time systematically, or—better still—averaging over momentum distributions  $f_{k,nn'}(t)$  before going on to compute final physical values [10].

In sum, the present results indicate that back-reaction in a finite volume allows for the replacement of the full field-theory calculation by the much simpler transport formalism at least at a loose, qualitative level for quantities averaged over the transverse direction. It is perhaps not surprising that the very close linkage between field theory and transport formalism found in the case of infinite volume [6-10] is lost here: The values of the radius  $R$  that we deal with are comparable with the particle mass, so that quantal effects should be expected to enter, and the spatial variability of the field is such that the “local” Schwinger form of Eq. (23) is not likely to prove adequate. This is in contrast to the infinite-volume situation [6-10], where the temporal variability of the physical quantities is measured by cycle times roughly an order of magnitude larger than  $R$  here.

This rough, qualitative correspondence between field theory and transport formalism may also apply for the physical quantities in greater detail as functions of the transverse parameter  $b$ , but present computer capabilities do not yet allow one to establish this. In all likelihood the correspondence will be strengthened somewhat by the consideration of the entire physical context, including particle interaction, irregular geometry, and the like. Thus for many practical purposes one may be able to replace a field-theory approach by a transport one at the level of qualitative behavior, and use the latter for further study of pre-equilibrium parton production.

It is a pleasure to acknowledge many valuable exchanges on the subject matter of this paper with Fred Cooper, Yuval Kluger, Emil Mottola, and Ben Svetitsky. At the start of the study I also had useful conversations on it with Gideon Dror and Stefan Graf. There were also helpful exchanges on this work at the Workshop on Parton Production and Transport in the Quark-Gluon Plasma held under the auspices of the European Centre for Theoretical Studies in Nuclear Physics and Related Areas (ECT\*) in Trento, Italy, in October 1994. This work was carried out with partial support from the U.S.-Israel Binational Science Foundation and from the Ne'eman Chair in Theoretical Nuclear Physics at Tel Aviv University.

## References:-

1. A. Białas and W. Czyż, Phys. Rev. D **30**, 2371 (1984); *ibid.* **31**, 198 (1985); Z. Phys. **C28**, 255 (1985); Nucl. Phys. **B267**, 242 (1985); Acta Phys. Pol. **B17**, 635 (1986).
2. G. Gattoff, A.K. Kerman, and T. Matsui, Phys. Rev. D **36**, 114 (1987).
3. S.A. Fulling, *Aspects of Quantum Field Theory in Curved Space-Time* (Cambridge University Press, Cambridge, 1989).
4. N.D. Birrell and P.C.W. Davies, *Quantum Fields in Curved Space* (Cambridge University Press, Cambridge, 1982).
5. Ya.B. Zel'dovich, in *Magic Without Magic: John Archibald Wheeler*, ed. J. Klauder (Freeman, San Francisco, 1972) p. 277.
6. Y. Kluger, J.M. Eisenberg, B. Svetitsky, F. Cooper, and E. Mottola, Phys. Rev. Lett. **67**, 2427 (1991).
7. Y. Kluger, J.M. Eisenberg, B. Svetitsky, F. Cooper, and E. Mottola, Phys. Rev. D **45**, 4659 (1992).
8. F. Cooper, J.M. Eisenberg, Y. Kluger, E. Mottola, and B. Svetitsky, Phys. Rev. D **48**, 190 (1993).
9. J.M. Eisenberg, Y. Kluger, and B. Svetitsky, Acta Phys. Pol. **B23**, 577 (1992).
10. Y. Kluger, J.M. Eisenberg, and B. Svetitsky, Int. J. Mod. Phys. E **2**, 333 (1993).
11. J. Schwinger, Phys. Rev. **82**, 664 (1951).
12. C. Best and J.M. Eisenberg, Phys. Rev. D **47**, 4639 (1993).
13. J. Rau, Phys. Rev. D, in press.
14. F. Cooper and Y. Kluger, private communication.
15. F. Cooper, S. Habib, Y. Kluger, E. Mottola, J.P. Paz, and P.R. Anderson, Phys. Rev. D **50**, 2848 (1994).
16. J. Ambjørn and S. Wolfram, Ann. Phys. **147**, 33 (1983).
17. F. Cooper and E. Mottola, Phys. Rev. D **40**, 456 (1989).



18. W.H. Press, B.P. Flannery, S.A. Teukolsky, and W.T. Vetterling, *Numerical Recipes* (Cambridge University Press, Cambridge, 1982).
19. Y. Kluger, private communication.

## Figure captions:-

FIG 1. Cylindrical geometry considered here. On the left side of the cylinder are shown typical actions of forces on negative and positive charges. Since charges of opposite sign are evenly distributed and their transverse motion is the same, they neutralize each other insofar as transverse contributions to the current are concerned.

FIG 2. Comparison between field-theory results (left-hand side) and transport theory calculation (right-hand side) for quantities integrated over the cylindrical cross section [i.e., transversely—see Eq. (27)]. Here the charge is  $e^2 = 10$ , the initial electric field on the cylinder axis is  $E(b = 0, t = 0) = 6$ , and the cylinder radius is  $R = 2$ , all in natural units (see Section IV).

FIG 3. Same as Figure 2, but for a cylinder radius  $R = 5$ .

FIG 4. Comparison between field-theory results (left-hand side) and transport theory calculation (right-hand side) for quantities on the cylinder axis. The charge is  $e^2 = 10$ , the initial electric field on axis is  $E(b = 0, t = 0) = 6$ , and the cylinder radius is  $R = 2$  in natural units (see Section IV).

FIG 5. Same as Figure 4, but for a cylinder radius  $R = 5$ .

FIG 6. Comparison between field-theory results (left-hand side) and transport theory calculation (right-hand side) for quantities integrated over the cylindrical cross section. Here the charge is  $e^2 = 4$ , the initial electric field on the cylinder axis is  $E(b = 0, t = 0) = 7$ , and the cylinder radius is  $R = 2$  in natural units.

FIG 7. Same as Figure 6, but for a cylinder radius  $R = 5$ .

FIG 8. Comparison between field-theory results (left-hand side) and transport theory calculation (right-hand side) for quantities on the cylinder axis. The charge is  $e^2 = 4$ , the initial electric field on axis is  $E(b = 0, t = 0) = 7$ , and the cylinder radius is  $R = 2$  in natural units (see Section IV).

FIG 9. Same as Figure 8, but for a cylinder radius  $R = 5$ .

FIG 10. Comparison between computation for integrated  $J(t)$ ,  $A(t)$ ,  $E(t)$  [see

Eq. (27)] using time interval  $dt = 10^{-4}$ , 1,001 longitudinal grid points, 20 Fourier-Bessel components ( $n_{max} = 20$ ), and cutoff  $\Lambda = 40$  taking several weeks (solid line) with a less accurate version having  $dt = 2 \times 10^{-4}$ , 401 grid points,  $n_{max} = 10$ , and  $\Lambda = 20$ , taking only a few days. The physical parameters here are the same as for Figure 2.

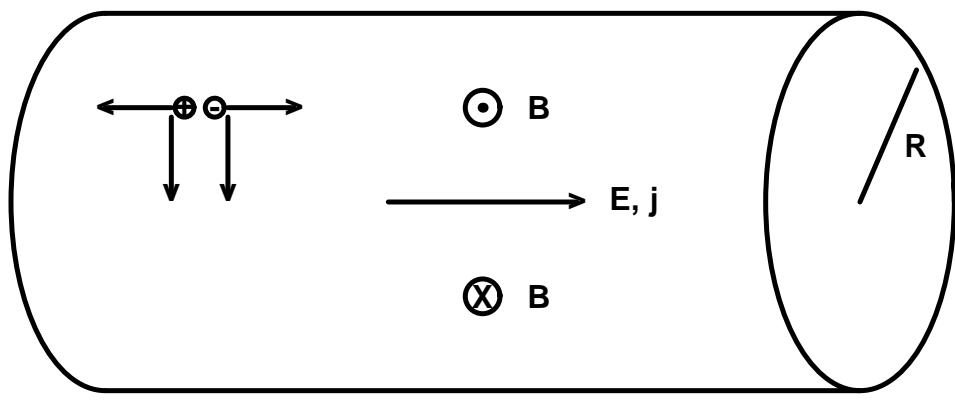
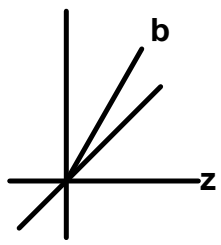
FIG 11. Same comparison as for Figure 10, but with cylinder radius  $R = 5$ .

FIG 12. Same comparison as in Figure 10, but for on-axis quantities  $j(b = 0, t)$ ,  $a(b = 0, t)$ ,  $e(b = 0, t)$ .

FIG 13. Same comparison as for Figure 12, but with cylinder radius  $R = 5$ .

This figure "fig1-1.png" is available in "png" format from:

<http://arxiv.org/ps/hep-ph/9410329v1>



This figure "fig2-1.png" is available in "png" format from:

<http://arxiv.org/ps/hep-ph/9410329v1>

This figure "fig3-1.png" is available in "png" format from:

<http://arxiv.org/ps/hep-ph/9410329v1>

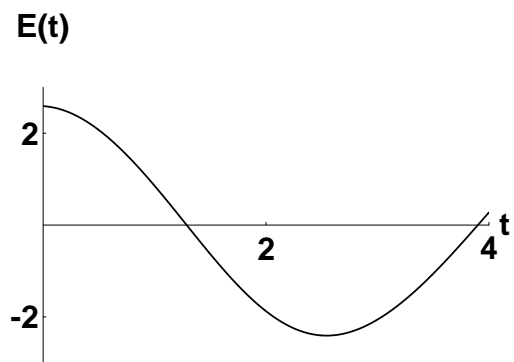
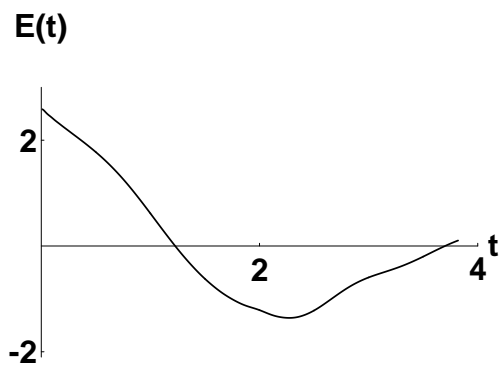
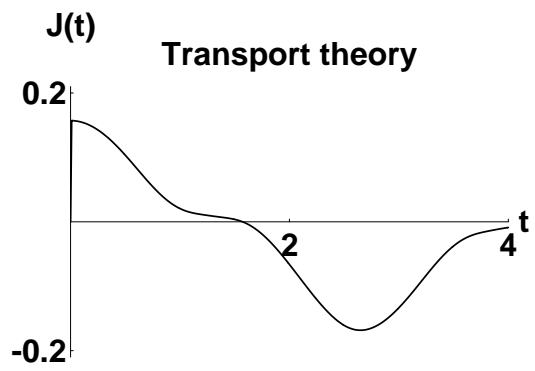
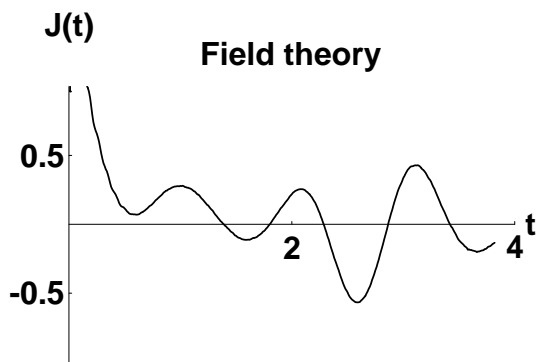
This figure "fig1-2.png" is available in "png" format from:

<http://arxiv.org/ps/hep-ph/9410329v1>



This figure "fig2-2.png" is available in "png" format from:

<http://arxiv.org/ps/hep-ph/9410329v1>



This figure "fig3-2.png" is available in "png" format from:

<http://arxiv.org/ps/hep-ph/9410329v1>

This figure "fig1-3.png" is available in "png" format from:

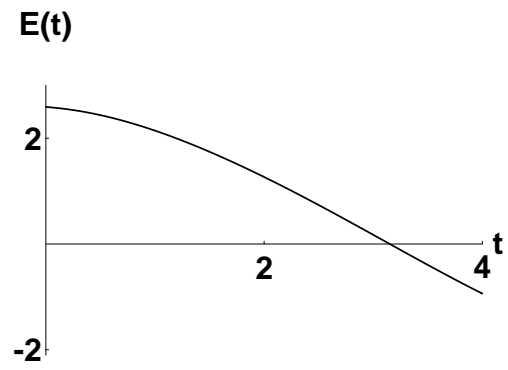
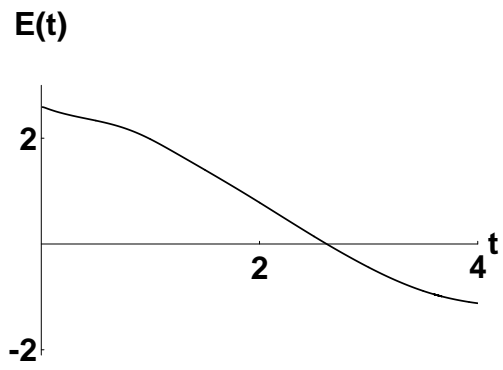
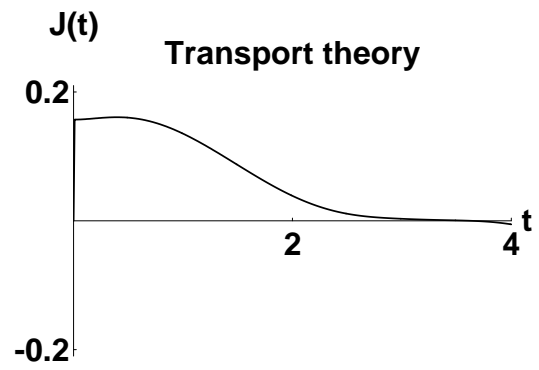
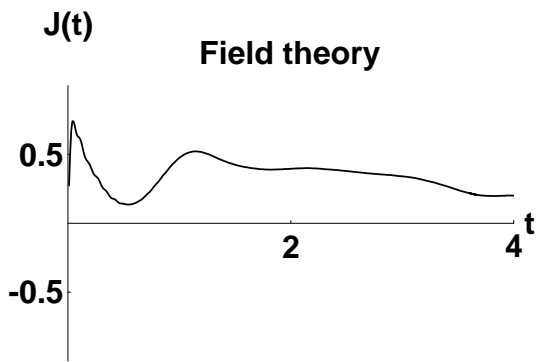
<http://arxiv.org/ps/hep-ph/9410329v1>

This figure "fig2-3.png" is available in "png" format from:

<http://arxiv.org/ps/hep-ph/9410329v1>

This figure "fig3-3.png" is available in "png" format from:

<http://arxiv.org/ps/hep-ph/9410329v1>



This figure "fig1-4.png" is available in "png" format from:

<http://arxiv.org/ps/hep-ph/9410329v1>

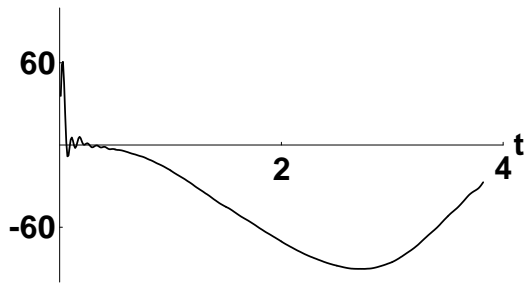


This figure "fig2-4.png" is available in "png" format from:

<http://arxiv.org/ps/hep-ph/9410329v1>

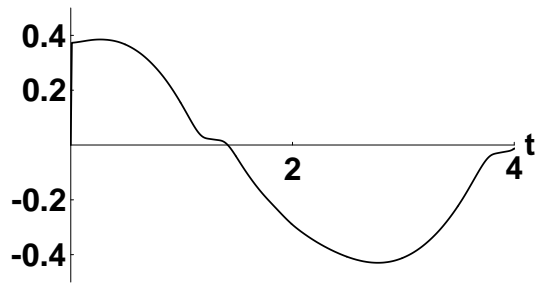
$j(0,t)$

Field theory

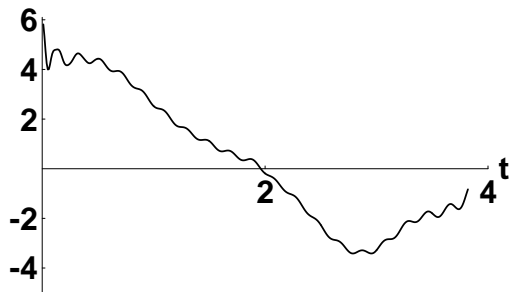


$j(0,t)$

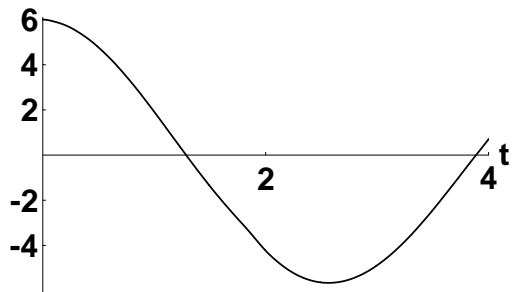
Transport theory



$e(0,t)$



$e(0,t)$

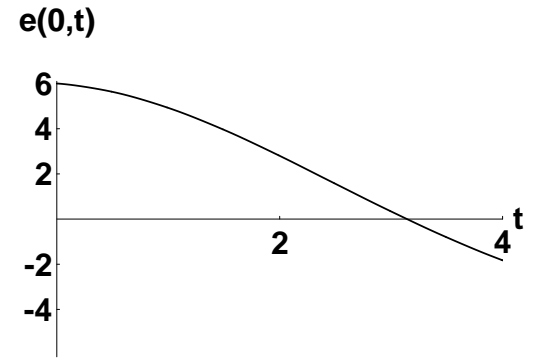
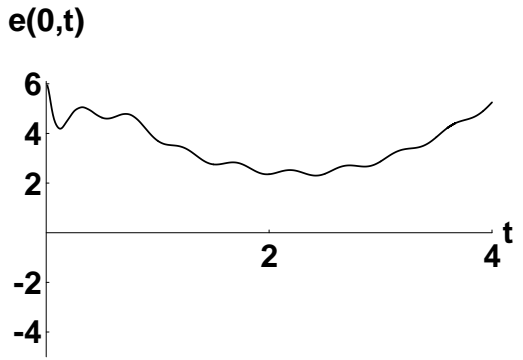
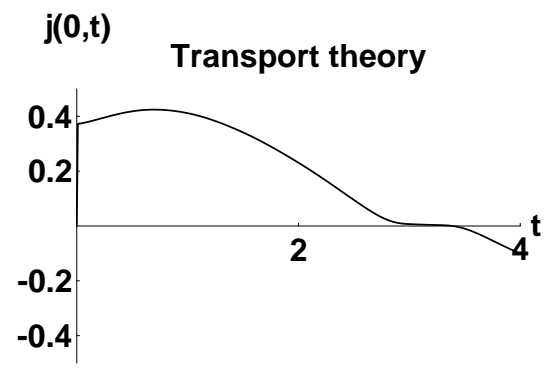
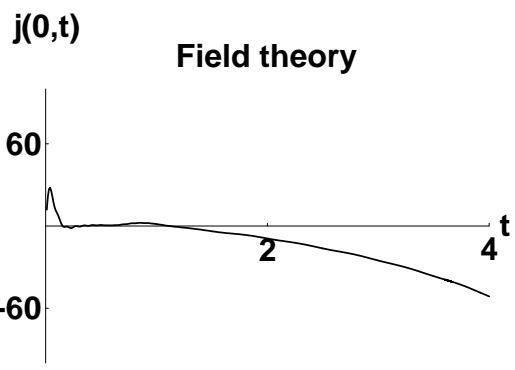


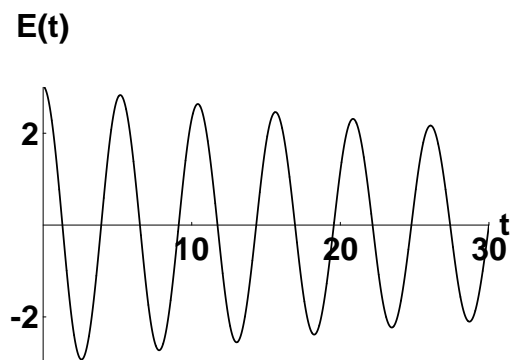
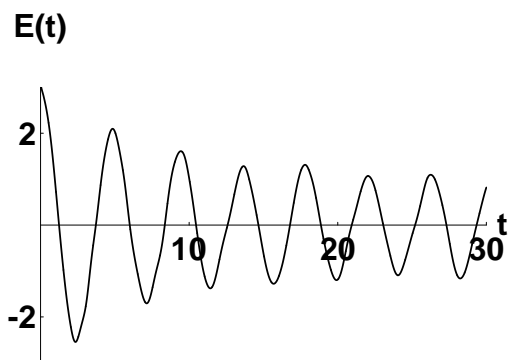
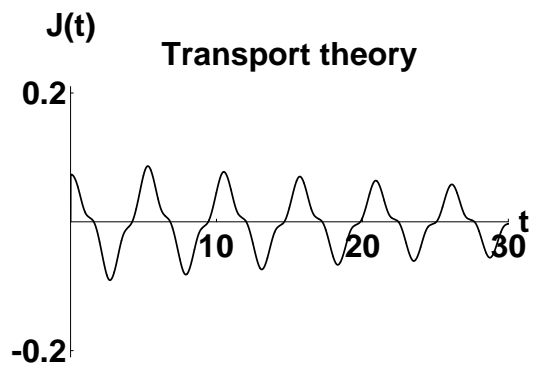
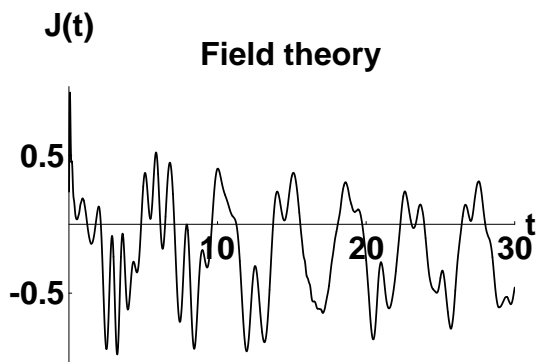
This figure "fig1-5.png" is available in "png" format from:

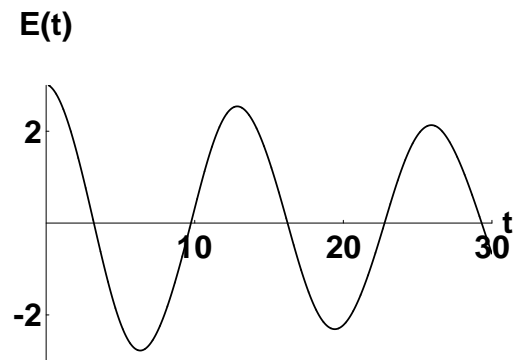
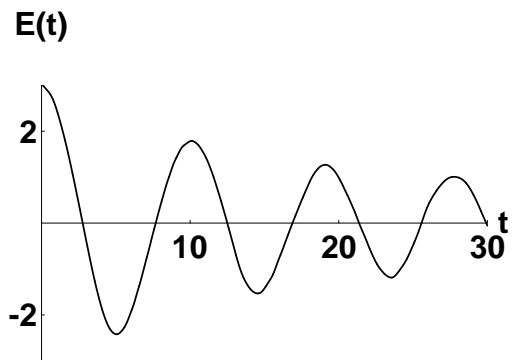
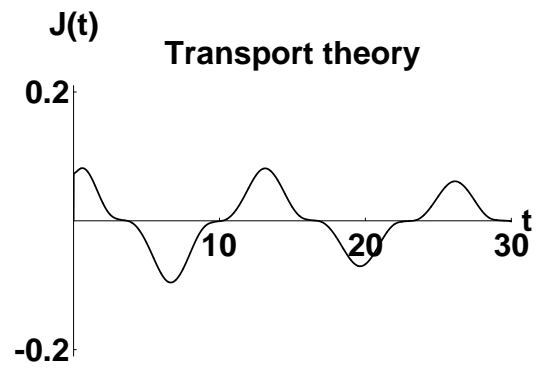
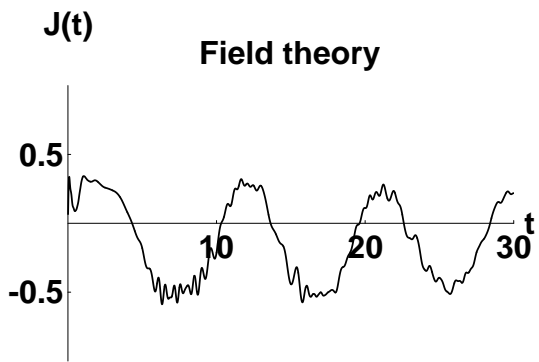
<http://arxiv.org/ps/hep-ph/9410329v1>

This figure "fig2-5.png" is available in "png" format from:

<http://arxiv.org/ps/hep-ph/9410329v1>

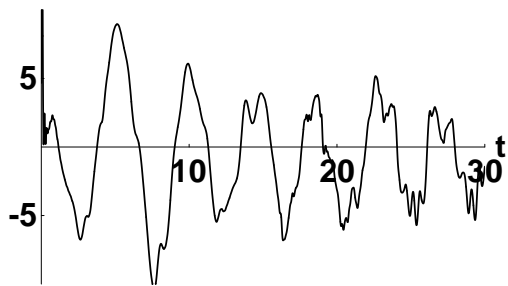






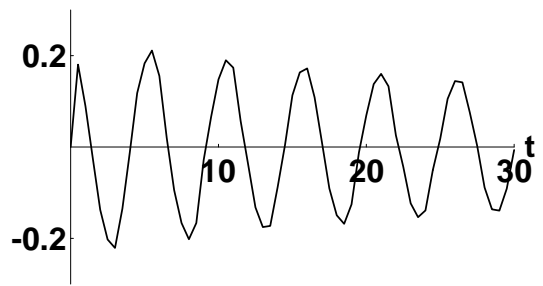
$j(0,t)$

Field theory

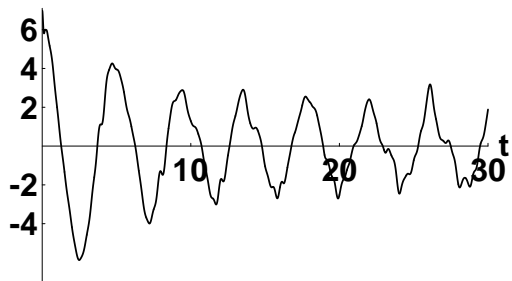


$j(0,t)$

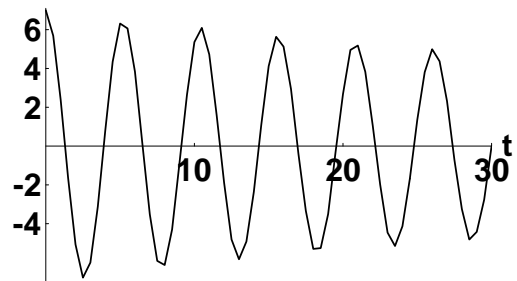
Transport theory



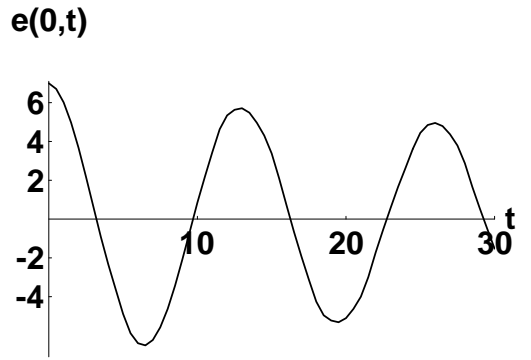
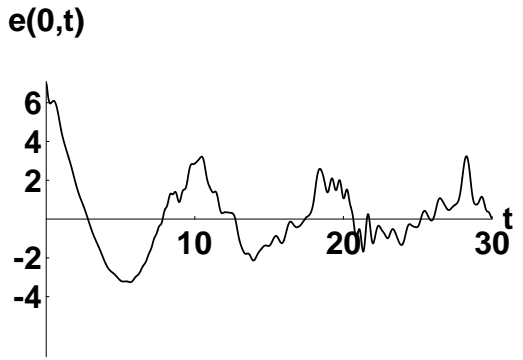
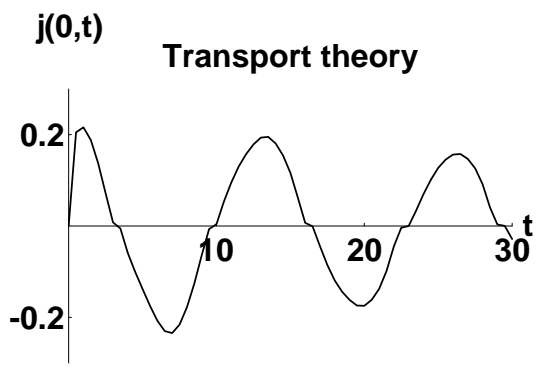
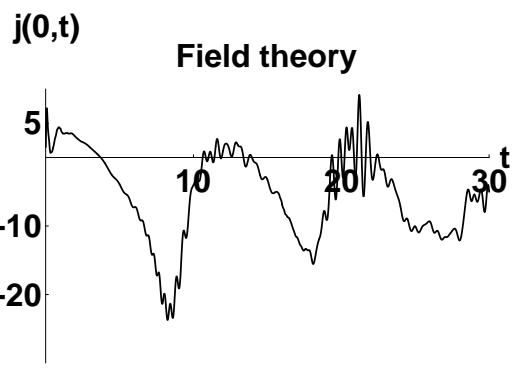
$e(0,t)$

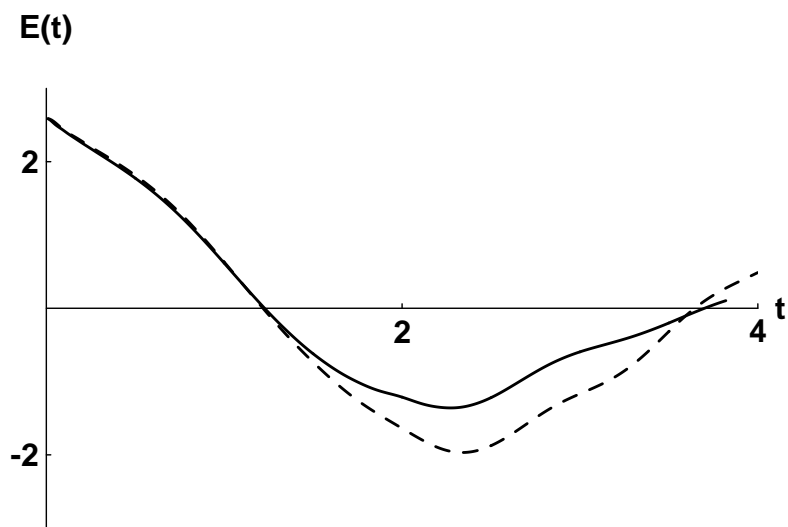
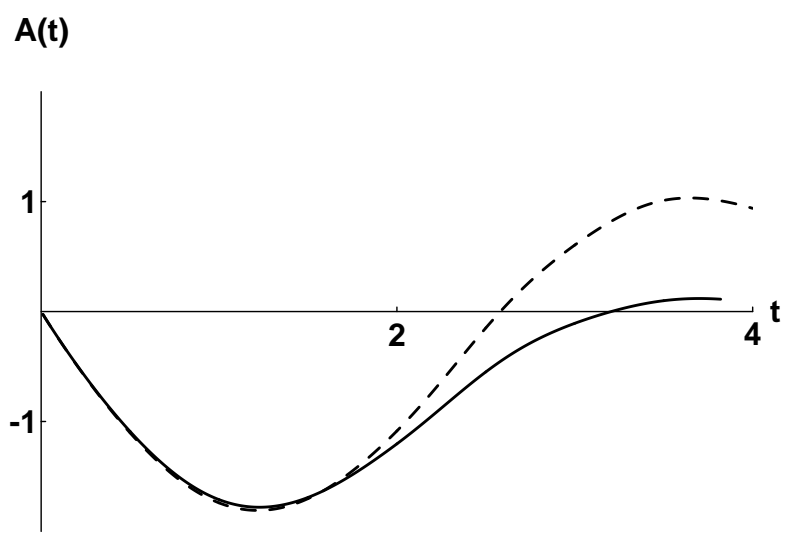
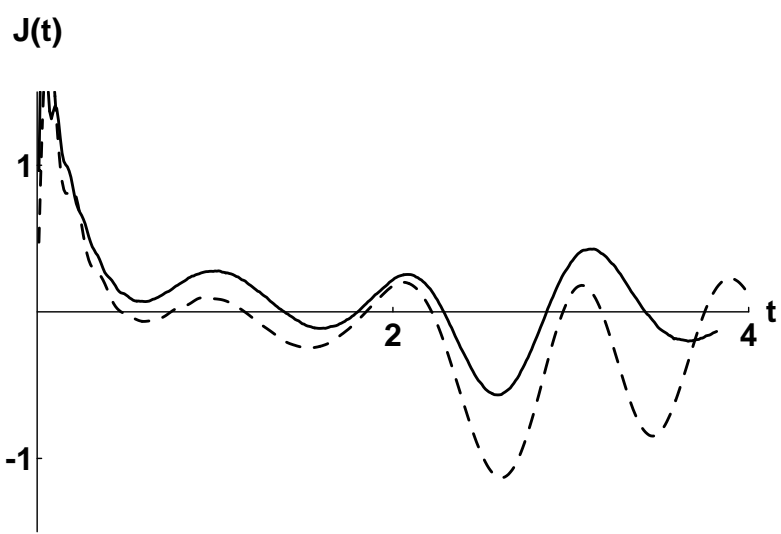


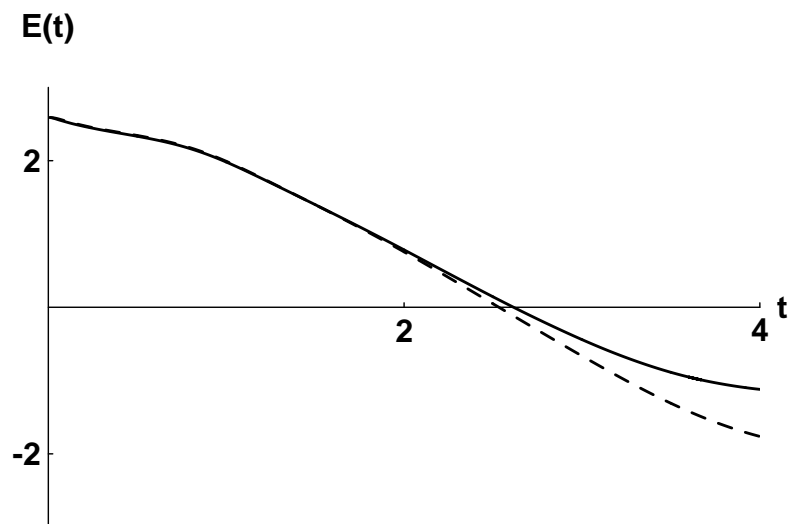
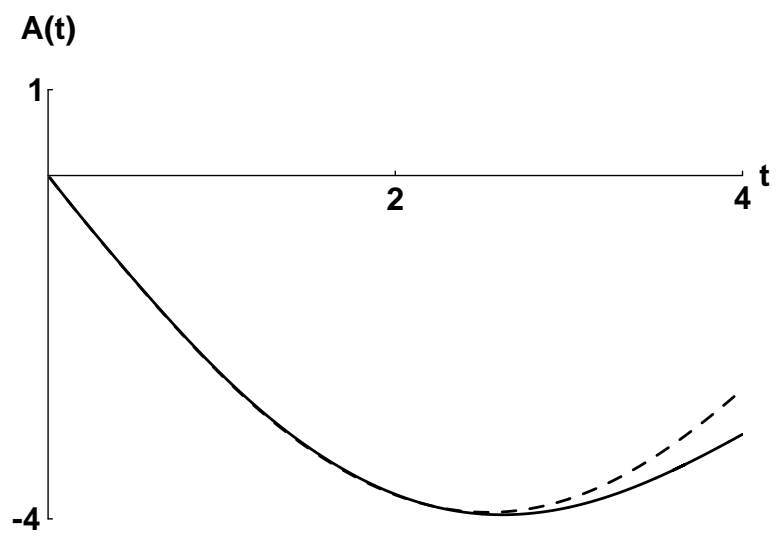
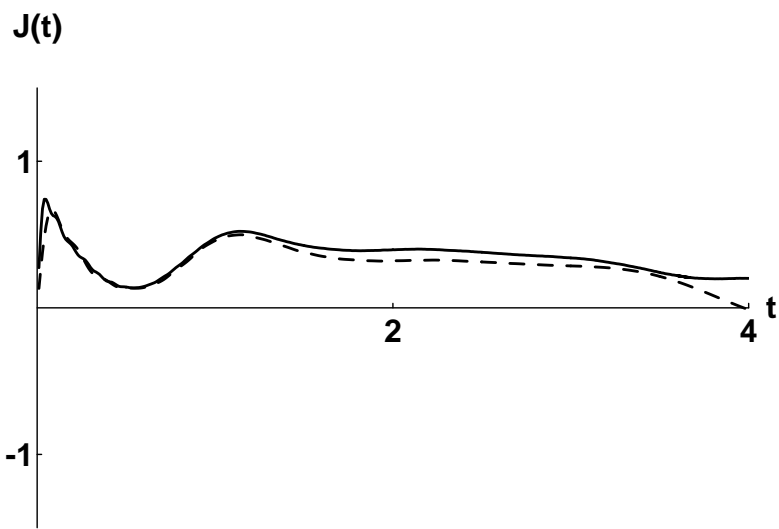
$e(0,t)$



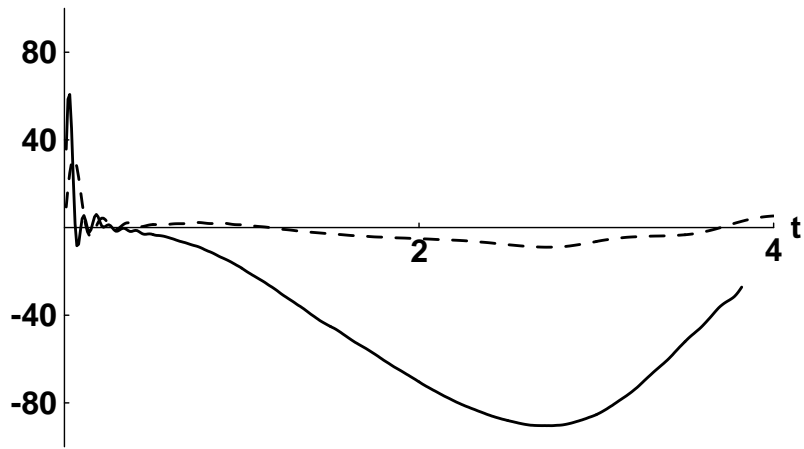




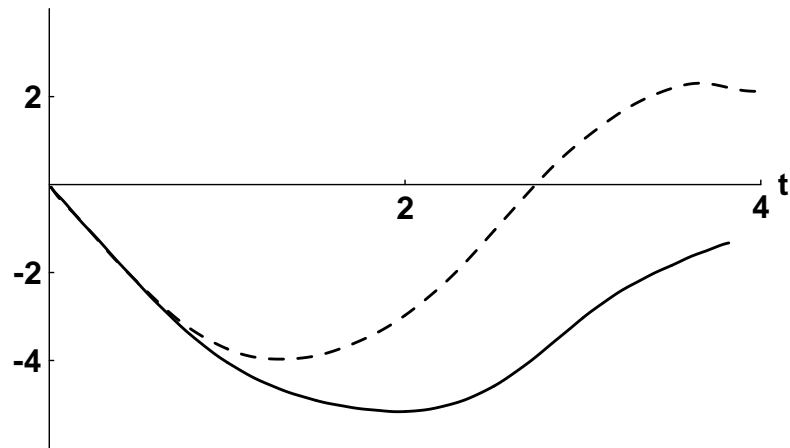




$j(0,t)$



$a(0,t)$



$e(0,t)$

